ISTITUTO NAZIONALE DI FISICA NUCLEARE
Laboratori Nazionali di Frascati

LNF-83/102

# P. Barreau et al. : DEEP-INELASTIC ELECTRON SCATTERING FROM CARBON

Estratto da:
Nuclear Phys. A402, 515 (1983)

Servizio Documentazione
dei Laboratori Nazionali di Frascati
Cas. Postale 13 - Frascati (Roma)

Nuclear Physics **A402** (1983) 515–540


# DEEP-INELASTIC ELECTRON SCATTERING FROM CARBON

P. BARREAU, M. BERNHEIM, J. DUCLOS, J.M. FINN[†],
Z. MEZIANI, J. MORGENSTERN, J. MOUGEY[††], D. ROYER, B. SAGHAI,
D. TARNOWSKI and S. TURCK-CHIEZE

*DPh-N/HE, CEN Saclay, 91191 Gif-sur-Yvette Cedex, France*

M. BRUSSEL[†††]

*Department of Physics, University of Illinois, Urbana, Illinois 61801, USA*

G.P. CAPITANI and E. DE SANCTIS

*Laboratori Nazionali di Frascati, INFN, 00044 Frascati, Italy*

S. FRULLANI and F. GARIBALDI

*Laboratorio della Radiazioni, Istituto Superiore di Sanità, Sezione Sanità,
Istituto Nazionale di Fisica Nucleare, Roma, Italy*

D.B. ISABELLE[‡]

*Laboratoire de Physique Corpusculaire, Université de Clermont II, Aubière, France*

E. JANS[‡‡]

*NIKHEF.-K, Amsterdam, The Netherlands*

I. SICK[‡‡‡]

*Department of Physics, University of Basel, Basel, Switzerland*

and

P.D. ZIMMERMAN[§]

*Louisiana State University, Department of Physics and Astronomy, Baton-Rouge, Louis. 70803, USA*

Received 5 October 1982
(Final version received 15 February 1983)

[†] Present address: MIT, LNS, Cambridge, Mass. 02139, USA.
[††] Present address: DRF/CPN, CEN Grenoble 85 X, 38041 Grenoble Cedex.
[†††] Supported in part by the US National Science Foundation.
[‡] Supported by Institut National de Physique Nucléaire et de Physique des Particules.
[‡‡] Supported by the Dutch Foundation for Fundamental Research on Matter (FOM).
[‡‡‡] Supported by the Swiss National Science Foundation.
[§] Supported by the US National Science Foundation and the Research Corporation.

**Abstract:** We have measured the deep-inelastic electron scattering from carbon up to and including the $\Delta$-region at 36°, 60°, 90° and 145°. The systematic decomposition of the transverse and longitudinal response functions has been obtained by means of a Rosenbluth-type analysis of the data in the momentum transfer interval $200\ \mathrm{MeV}/c < |q| < 600\ \mathrm{MeV}/c$. A comparison with theoretical calculations which extend over the quasielastic and $\Delta$-peak regions is presented. A reduction of the differences between our data and theory seems obtainable through the introduction of meson-exchange currents, resonant and non-resonant meson production, and the use of the shell model. Our experimental Coulomb sum-rule estimates at higher $|q|$ agree with independent particle model predictions. We compare our results in the vicinity of the $\Delta$-peak with the total absorption cross section for real photons.

E NUCLEAR REACTIONS C(e, e'), $E = 120$–$680$ MeV; measured $\sigma(\theta, E, E')$; deduced sum rule. Response functions decompositions $q = 200$–$600\ \mathrm{MeV}/c$.

## 1. Introduction

Many of the properties of nuclei are well explained by models embodying only two-body interactions between nucleons considered as elementary particles. Despite the general success of these models, they are too simple to describe precisely such basic quantities as binding energies, nuclear densities and electromagnetic moments. Inclusive deep-inelastic electron scattering (e, e') experiments illustrate the current situation well. In electron–nucleus scattering at high momentum transfer ($|q| > 400\ \mathrm{MeV}/c$), one finds a characteristic peak in the scattered electron energy spectrum, whose position corresponds (almost) to the scattering from free nucleons at rest and whose width reflects the internal motions of those nucleons in the target nucleus. This is called the quasielastic peak. At higher energy loss, other peaks are observed. These may be identified with the excitation of (free) nucleon resonance. A close examination of measured spectra, however, reveals discrepancies with calculations based on simple models, especially in kinematic regions which are sensitive to high nucleon momentum components in the nucleus. One such region is the tail of the quasielastic peak. As examples, one may cite the (e, e') survey experiment of Whitney *et al.* [1]) on nine nuclei, where an excess of cross section was observed for energy losses greater than that of the quasielastic peak. Similar results were reported for $^3$He [ref. [2])], $^{12}$C [ref. [3])] and $^{40}$Ca [ref. [4])]. In all these cases, an insufficiency of high momentum components in the theoretical nuclear wave function has been offered [5]) as an explanation, but this may not be quantitatively sufficient.

Meson currents are expected to play an explicit role here, the virtual photon coupling directly, or indirectly through resonances, to the meson field which is presumed to exist in the nucleus. Thus, deep-inelastic (e, e') experiments would seem to be able to reveal the nature and importance of extra-nucleonic processes in nuclei above, but also below, the pion production threshold. It was with this expectation, together with a continuing desire to study in more detail the specifically

nucleonic degrees of freedom in the nucleus, that the present experiment was undertaken.

## 2. The experiment

The measurements reported here on the $^{12}C(e, e')^{\dagger}$ reaction at high inelasticities were made using the electron scattering facilities of the Saclay Linear Accelerator (ALS). This work extends a previous Saclay experiment [3]) on this reaction into the delta region and permits the decomposition of the response function into its longitudinal and transverse components over an extended region of momentum transfer (see sect. 3). Such a decomposition should allow the disentangling of various effects contributing to the cross section. The transverse response function is very sensitive to mesonic effects while the longitudinal response is relatively free of such ambiguities. Thus, from the longitudinal response function, the nucleon momentum distribution can be extracted with greater confidence; however it is difficult to obtain the longitudinal response function with good accuracy. In this experiment, special care has been taken to subtract the background; the pion background was eliminated using a gas Čerenkov counter and electron pair production systematically measured. Under these conditions, the Coulomb "sum rule" [6]) can be tested. A test of this sum rule is particularly interesting, because recent results from $^{56}Fe$ [ref. [7])] have shown large differences between experimentally determined values of the sum-rule integrals of the longitudinal response functions and those predicted by a Fermi-gas model calculation [8]).

Conversely, by using the longitudinal response to determine the pure nucleonic strength, the transverse response function can be examined to see the importance of the meson currents and the nature of the nucleon resonances as they appear in the nuclear medium.

In the present experiment, data were obtained at bombarding energies between 120 MeV and 680 MeV and at scattering angles of 36°, 60°, 90° and 145°. In consequence, Rosenbluth decompositions could be made at momentum transfers up to 600 MeV/$c$. The highest momentum transfer obtained is considerably more than twice the nuclear Fermi momentum [$k_F = 220$ MeV/$c$; ref. [1])] expected from $^{12}C$, so that nuclear structure effects such as Pauli blocking should be small.

## 3. Kinematics

The laboratory kinematics for electron scattering can be represented by the diagram of fig. 1. $E$ represents the incident electron energy, $E'$ the energy of the scattered electron, $\omega = E - E'$ the energy transfer, and $\theta$ the scattering angle; the

† In fact, the targets used in the Saclay measurements were of natural carbon. The $^{13}C$ contribution being negligible for our purposes, we shall signify the target as $^{12}C$.

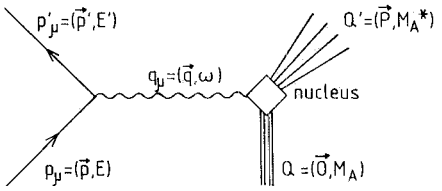


Fig. 1. Schematic diagram of electron inelastic scattering. $(\boldsymbol{p}, E)$ and $(\boldsymbol{p}', E')$ are the momentum 4-vectors for the incident and scattered electrons, respectively. The momentum transfer 4-vector $q_\mu = (\boldsymbol{q}, \omega)$ represented as a single virtual photon, changes the state of the initial nucleus $A$ to the final state $A^*$.

momentum transfer, $\boldsymbol{q} = \boldsymbol{p} - \boldsymbol{p}'$, and the four-momentum transfer, $q_\mu$, are given by the following equations:

$$\begin{aligned} \boldsymbol{q}^2 &= E^2 + E'^2 - 2EE' \cos\theta\,, \\ q_\mu^2 &= 4EE' \sin^2 \tfrac{1}{2}\theta, \\ &= \boldsymbol{q}^2 - \omega^2\,. \end{aligned}$$

Subsequently, we shall write $q \equiv |\boldsymbol{q}|$. (We ignore the negligible electron mass in these expressions.)

Measurements of the cross sections at fixed values of $(q, \omega)$ but at different scattering angles $(\theta)$ allow the values of the response functions $R_L(q, \omega)$ and $R_T(q, \omega)$ to be obtained by means of a Rosenbluth plot. $R_L$ and $R_T$, the response functions for longitudinally and transversely polarized virtual photons, can be obtained from the measured differential cross sections and the Mott cross sections, $\sigma_M$, by use of the expression

$$\frac{\mathrm{d}^3\sigma}{\mathrm{d}\Omega\,\mathrm{d}\omega} \Big/ \sigma_M \equiv R(q, \omega, \theta) = \left\{ \left(\frac{q_\mu}{\boldsymbol{q}}\right)^4 R_L(q, \omega) + \left[ \frac{1}{2}\left(\frac{q_\mu}{\boldsymbol{q}}\right)^2 + \mathrm{tg}^2 \tfrac{1}{2}\theta \right] R_T(q, \omega) \right\}, \quad (1)$$

where

$$\sigma_M = \frac{\alpha^2}{4E^2} \frac{\cos^2 \frac{1}{2}\theta}{\sin^4 \frac{1}{2}\theta} \qquad (\alpha = e^2 = \tfrac{1}{137})$$

in units where $\hbar = c = 1$.

This formula is derived in the framework of the first Born approximation, and is justified for use with the $^{12}$C nucleus, as will be shown below. $R(q, \omega, \theta)$ is called the total response function.

In fig. 2, we show the regions of the $(q, \omega)$ plane where measurements were made (A and B) and where $R_L$ and $R_T$ have been determined (B). No measurements were made in region C.

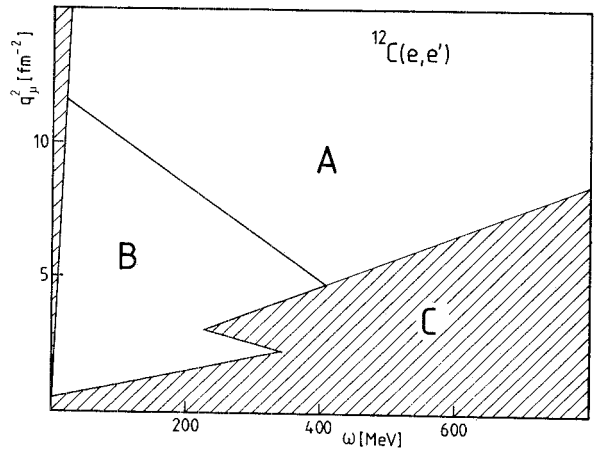


Fig. 2. Region of the $(q_\mu, \omega)$ plane where measurements were made (A and B) and where $R_L$ and $R_T$ have been extracted (B). C is the region where no measurements were made.

## 4. Experimental equipment and procedure

### 4.1. EQUIPMENT

The experiment was performed at the linear accelerator of Saclay using the "600" spectrometer in the HE1 end station. The detector array in the focal plane of the spectrometer consisted of two multiwire proportional counter chambers, a plane of plastic scintillators ("R" counters) and a set of Čerenkov detectors ("C" counters). This apparatus is described in detail in ref. [9]).

For this experiment it was crucial to reject pions produced in the target. Therefore, Čerenkov detectors made of silica aerogel [10]), whose refractive index ($n = 1.06$) was lower than that of the Čerenkov detectors of ref. [9]), were used for most of the measurements. Pions of momentum less than 0.4 GeV/$c$ were consequently rejected. The electron detection efficiency was measured to be 98%. However, these detectors manifested high background counting rates from ambiant gamma rays. They were therefore replaced (for all 36° and 60° data and for $E > 480$ MeV) by a gas Čerenkov detector filled with freon-114 at atmospheric pressure. Because this gas had a refractive index of $n = 1.00135$, and the detector constructed had directional sensitivity, a background counting rate reduced by a factor of five was obtained relative to the aerogels. Fig. 3 shows its typical pulse-height spectrum, and implies that more than 13 photoelectrons per detected event were produced in the PM tubes. The efficiency for electron detection was greater than 99%, and pions of momenta less than 2.7 GeV/$c$ were eliminated.

A valid event was signified by a trigger pulse formed by a coincidence between a plastic scintillator (R) and the appropriate Čerenkov (C) detector. Shown in

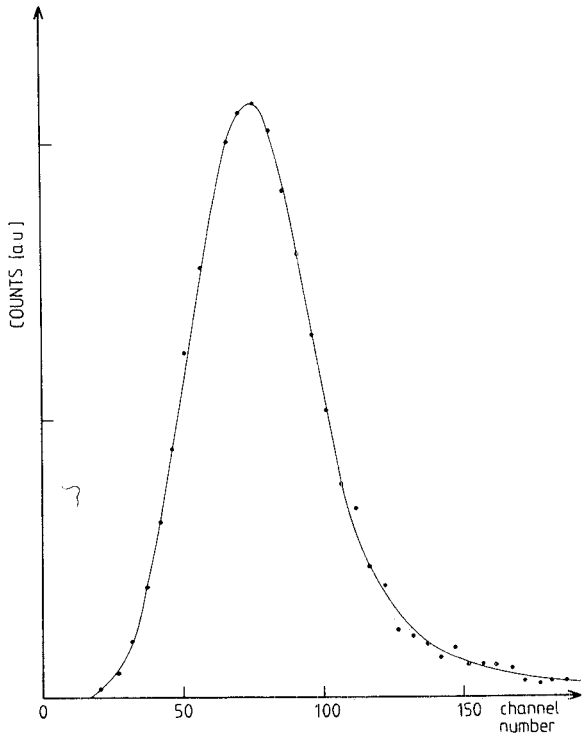


Fig. 3. Pulse-height spectrum obtained from freon gas (1 atm) Čerenkov detector. The curve represents a fit to the data for a Poisson distribution corresponding to 13 photoelectrons.

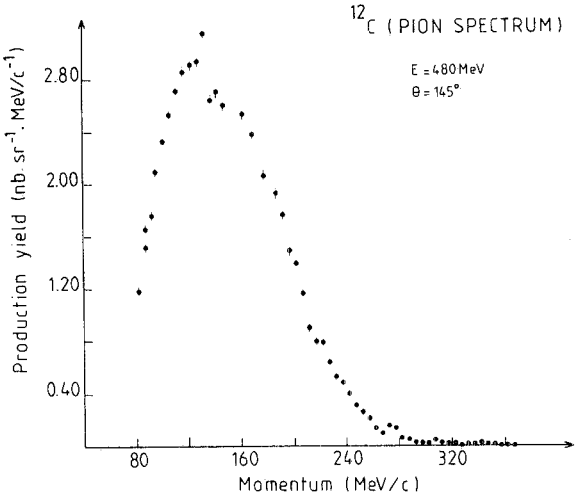


Fig. 4. Pion momentum spectrum obtained with the gas Čerenkov counter in anticoincidence to eliminate electron events.

fig. 4 is the pion spectrum obtained with C in anticoincidence with R. This anticoincidence condition eliminated electron events. When the trigger was formed normally, real pion events were eliminated, but accidental coincidences between pions detected in R and background electrons detected in C could still occur. In this way, a pion contribution to the measured spectrum could appear at momenta between 80 and 300 MeV/$c$. In order to be able to correct for such events, pion spectra systematically were measured, and the rate of accidental coincidences was continuously monitored. The accelerator beam current was adjusted so as to limit the correction due to this type of accidental event to less than 5%. Dead time corrections were typically between 0.5% and 1.5%.

This background from accidental pions was not measured in the previously published data [3]). Hence uncertainties exist for the data reported there in the energy region where a pion contribution can occur. This contribution was 20% of the measured cross section at $E = 480$ MeV and $\theta = 130°$. Therefore, we have elected not to use the 130° data in determining separated response functions. On the other hand, the errors from accidental pion events in the older 60° data are much smaller and could safely be neglected. These data have been included in the present work.

The spurious contribution of electrons from pair production in the target was measured by reversing the magnetic field of the spectrometer in order to detect positively charged particles. An effect of several percent of the deep-inelastic cross section was found at low final positron momenta, as shown in fig. 5. Simple analytic fits to the measured positron spectrum were made, and a corresponding number of events was subtracted from the electron spectra, assuming equal positron and electron production rates and spectrum shapes.

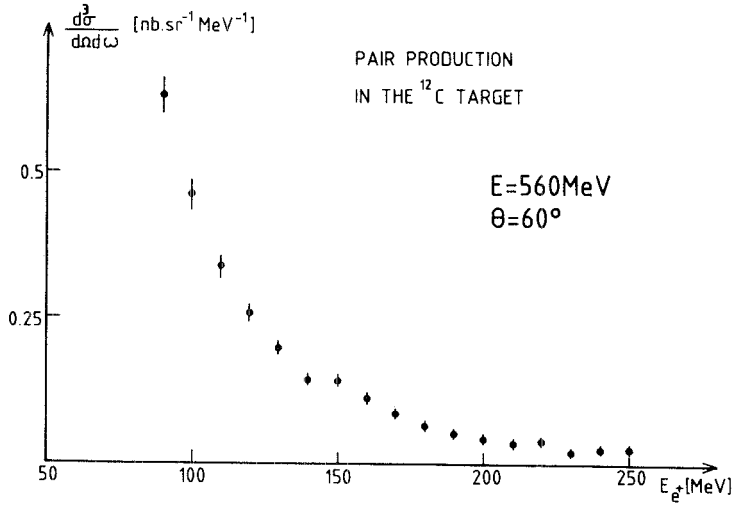


Fig. 5. Positron spectrum illustrating the contribution of electrons pair-produced in the target.

The efficiency of our detection system was determined in two stages. In one stage, the *relative* efficiencies corresponding to the individual wires of the multiwire proportional counter were determined by making several measurements in the smooth part of the quasi-elastic spectrum and fitting a polynomial to the data. In a second stage, the *absolute* efficiency of the system was determined by measuring the carbon elastic peak at several incident electron energies between 120 MeV and 560 MeV. For momentum $q \approx 1\,\mathrm{fm}^{-1}$ the data were compared to the absolute measurements made at NBS [11]) and Mainz [12]). Measurements near the second maximum of the elastic scattering form factor (at $\approx 2\,\mathrm{fm}^{-1}$) were compared to the Mainz data. The efficiency of the system at a fiducial point of the focal plane was found to be constant as a function of field setting for electrons of momenta above 300 MeV/$c$. It decreased slightly for lower momenta as shown in fig. 6. To take account of the uncertainties in the efficiency, a systematic error varying from 2% near 300 MeV/$c$ to 5% at 100 MeV/$c$ was included on the estimate of the total experimental uncertainty.

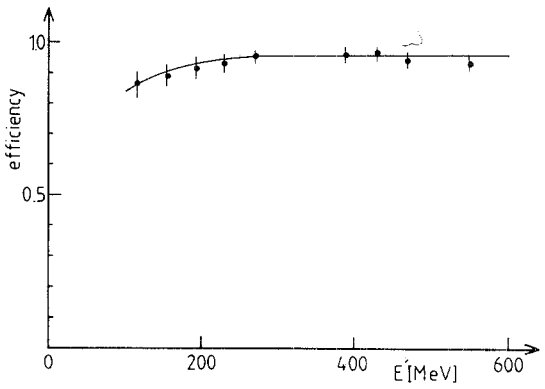


Fig. 6. Efficiency of the "600" spectrometer detector system as a function of scattered electron energy $E'$. The solid curve is simply a curve drawn through the data points.

## 4.2. PROCEDURE

For each measurement at each angle and incident energy, several (three to ten) values of spectrometer magnetic field setting were needed to cover the total energy range of the scattered electrons. The wire chambers in the spectrometer focal plane cover a region in $\Delta p/p$ (momentum fraction) equal to 32.5%. However, because of the uneven efficiency at the ends of the chambers due to the geometrical shape of the Čerenkov counter, the useful and effective part of the $E$-chamber has a reduced, 26.5%, momentum acceptance.

## 5. Radiation-corrected cross sections

In any electron scattering process, the electron loses additional energy by the radiation of (real or virtual) photons not associated with the nuclear transition. As a result, the electron spectrum which is measured can differ appreciably from the one which would have been produced, in the absence of this radiation, by the processes one wishes to study. The radiative corrections may be divided into two classes depending on whether or not the scattering nucleus absorbs excitation energy. Thus, for a given energy loss in the detected electron spectrum, one must (a) subtract the radiative tail of the elastic electron-nucleus scattering, and (b) perform an unfolding procedure to obtain the appropriate corrections for the inelastic (continuum) part of the spectrum. The latter corrections can be satisfactorily treated using the peaking approximation [13]); this approximation cannot be used to compute the radiative tail.

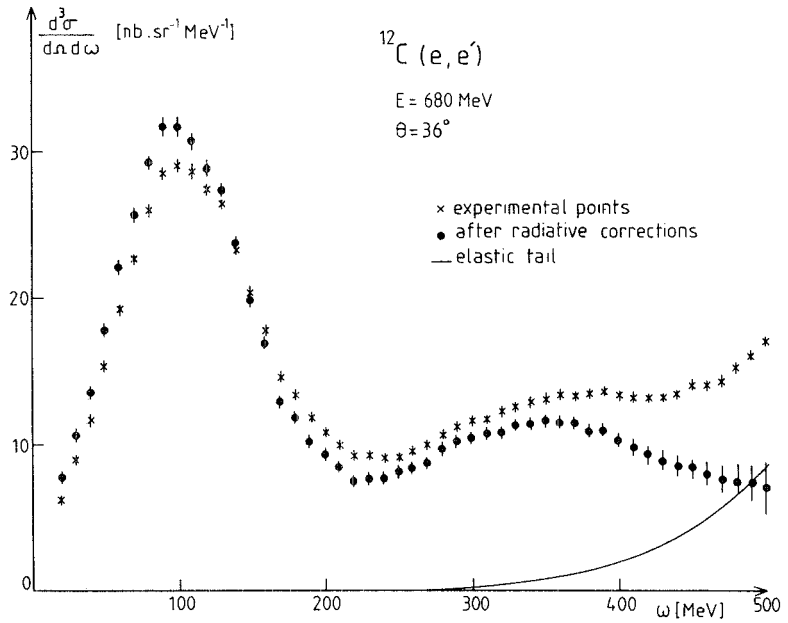


Fig. 7. Radiative effects in deep-inelastic scattering. The experimental data and the radiatively corrected data are shown, together with the calculated elastic radiative tail.

The effects of the radiative corrections are shown in fig. 7. The radiative tail is seen to be important only at large energy losses, while the effect of radiation by non-elastically scattered electrons is to shift the quasielastic peak to larger energy losses and to alter somewhat the distribution of strength of the cross section.

5.1. PROCEDURE

The radiative tail has been calculated following the procedure given by Tsai [14]) with the formalism of Mo and Tsai [15]). This calculation does not use the peaking approximation and integrates over all photon emission angles. It includes the effects of virtual photon and multiple soft real photon emission. A comparison was made with a recent method of Chahine [16]) and good agreement was found in the region of interest. However, both methods use the first Born approximation. Thick-target bremsstrahlung was also accounted for. No correction for Landau straggling was made, as it is negligible in the region where the elastic radiative tail is significant.

A three-parameter Fermi fit to the charge distribution [17]) was used to compute the (carbon) elastic scattering form factor. The radiative tail only becomes a significant contribution to the cross section at large energy losses, where it is largely due to electrons which radiate before scattering. As a result, the radiative tail is almost insensitive to the details of the form factor used, as long as the latter yields the correct RMS charge radius. This assertion was tested by recalculating the tail using a harmonic oscillator form factor which gave the same RMS radius as the Fermi distribution. The results differed by less than one percent even in the low-energy region of the scattered electrons where the tail is large.

The error made in using the first Born approximation to compute the elastic radiative tail, was estimated from E. Borie's second Born calculation [18]). Here the calculation is strictly valid only for a point nucleus, and applies only to the peaking part of the radiative tail [19]). It is, nevertheless, a measure of the uncertainty which arises from the consistent use of the first Born approximation both for scattering and radiative processes. For $Z=6$ the Borie term is about 6% of the calculated radiative tail at a 90° scattering angle, and varies as $\{\sin(\frac{1}{2}\theta)[1+\sin(\frac{1}{2}\theta)]^{-1}\}$. This estimate was added to the experimental uncertanties after the subtraction of the tail and before the unfolding of the data. When the calculated size of the radiative tail exceeded 50% of the measured cross section, the data in that region were excluded from further analysis.

After the radiative tail was subtracted from the measured deep-inelastic scattering spectra, these spectra were then unfolded following the techniques of Mo and Tsai as elaborated upon by Miller [13]). This treatment includes the effects of multiple soft photon emission and thick target straggling, and is an effective radiator approximation.

In principle, in order to find the true (e, e') cross section for given incident ($E_0$) and scattered ($E_0'$) energies, one must know the cross sections for all incident energies $E$ such that $E_0' < E < E_0$ and for all scattered energies $E'$ such that $E_0' < E' < E_0$. In a practical experiment, the necessary cross sections must be obtained by interpolation from a limited number of points. Such a procedure has proven to be reliable and to converge rapidly. In this experiment, spectra were taken generally at 40 MeV incident energy intervals, although it was found that at

TABLE 1

List of the kinematical parameters corresponding to our measured cross sections (the complete list of the radiation corrected cross sections can be obtained in ref. [37]))

| $\theta = 36°$ | | $\theta = 60°$ | | $\theta = 90°$ | | $\theta = 145°$ | |
|---|---|---|---|---|---|---|---|
| $E$ (MeV) | minimal $E'$ (MeV) | $E$ (MeV) | minimal $E'$ (MeV) | $E$ (MeV) | minimal $E'$ (MeV) | $E$ (MeV) | minimal $E'$ (MeV) |
| 680.00 | 177.50 | 680.00 | 132.50 | 556.80 | 287.50 | 560.00 | 97.50 |
| 620.00 | 177.50 | 620.00 | 122.50 | 519.30 | 287.50 | 479.40 | 107.50 |
| 560.00 | 177.50 | 560.00 | 117.50 | 479.40 | 107.50 | 440.00 | 102.50 |
| 480.00 | 172.50 | 518.80 | 147.50 | 400.50 | 102.50 | 399.70 | 100.00 |
| 400.00 | 242.50 | 479.80 | 137.50 | 360.10 | 100.00 | 360.10 | 100.00 |
| 320.00 | 227.50 | 440.00 | 162.50 | 320.70 | 102.50 | 320.10 | 100.00 |
| 240.00 | 177.50 | 401.00 | 132.50 | 280.10 | 102.50 | 280.10 | 102.50 |
| 200.00 | 152.50 | 360.90 | 132.50 | 241.10 | 102.50 | 241.10 | 102.50 |
| 160.00 | 132.50 | 320.30 | 152.50 | 199.90 | 100.00 | 199.90 | 100.00 |
| | | 280.30 | 142.50 | 159.70 | 97.50 | 159.70 | 97.50 |
| | | 240.40 | 132.50 | 119.60 | 97.50 | 119.60 | 97.50 |
| | | 200.00 | 132.50 | | | | |
| | | 160.90 | 111.50 | | | | |

higher bombarding energies the results were relatively insensitive to the inclusion of lower energy spectra due to the slow variation of the nuclear response function.

### 5.2. RESULTING CROSS SECTIONS

In table 1 we present a list of the energies and angles where the cross sections were measured.

## 6. Longitudinal and transverse response functions

### 6.1. GENERAL REMARKS

In the first Born approximation, (e, e′) differential cross sections can be divided into contributions from longitudinally and transversely polarized virtual photons. These contributions yield the longitudinal and transverse response functions $R_L(q, \omega)$ and $R_T(q, \omega)$ previously defined. Measurement of $d^3\sigma/d\Omega\, d\omega$ at constant values of $q$ and $\omega$ but at two different scattering angles provide sufficient information to extract the two response functions. However, measurements at additional scattering angles are useful in checking the internal consistency of the data, in reducing the uncertainty in the values obtained for the response functions, and in verifying the applicability of the first Born approximation.

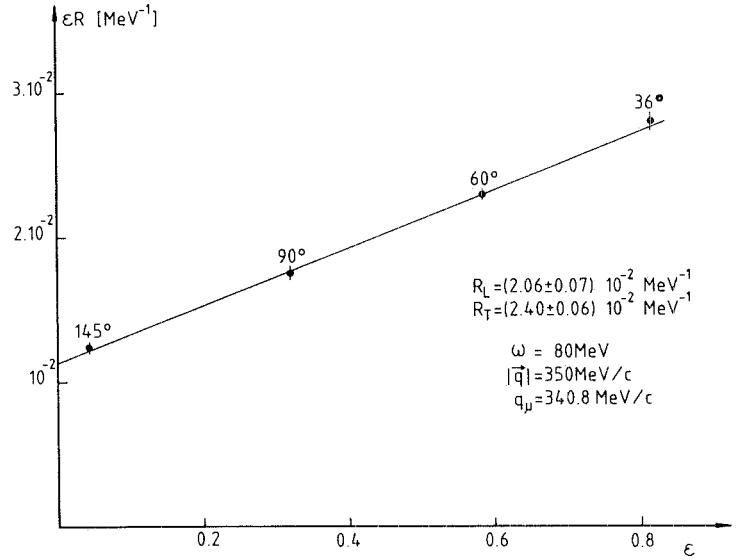


Fig. 8. Example of a Rosenbluth plot. For definition of the polarization parameter $\varepsilon$, and the response functions, see the text.

$R_L(q, \omega)$ and $R_T(q, \omega)$ are found by plotting the total response function, $R(q, \omega)$ against $[(q_\mu^2/2q^2)+\mathrm{tg}^2(\frac{1}{2}\theta)]$. In this case, the slope is proportional to $R_T(q, \omega)$ and the intercept to $R_L(q, \omega)$. The precision with which $R_L$ can be extracted is, however, better illustrated by plotting $\varepsilon R(q, \omega)$ versus $\varepsilon$, where $\varepsilon$ is the polarization parameter [20]) given by $\varepsilon = [1+(2q^2/q_\mu^2)\,\mathrm{tg}^2(\frac{1}{2}\theta)]^{-1}$. In this representation, the slope of $\varepsilon R$ is proportional to $R_L$. Therefore, the precision of $R_L$ is set by the difference between the largest and smallest values of $\varepsilon$. The maximum energy available at the ALS permits choosing the most forward scattering angles small enough to give an interval in $\varepsilon$ of at least 0.5. A typical plot of this kind is shown in fig. 8. The four experimental points are well aligned and so justify our use of the first Born approximation in $^{12}$C.

### 6.2. TRANSVERSE/LONGITUDINAL DECOMPOSITIONS

Depending on the values of $q$ and $\omega$, two, three or four angles have been used to determine $R_L$ and $R_T$. The following technique was used. The measured cross sections were first divided by the Mott cross sections. This yielded a slowly varying total response function, $R(q, \omega, \theta)$. To obtain values of $R$ at points between the measured energy spectra, a linear interpolation was used along lines of constant $\omega/E$. This variable is an attractive one: it lies between 0 and 1, and $R(\omega/E)$, at fixed $\theta$ and $q$, was observed to vary slowly. The use of parabolic interpolation did not lead to a significant improvement over the linear interpolation. Moreover it had a tendency to amplify small fluctuations in the data.

The longitudinal and transverse response functions in the quasielastic peak have been determined for constant $q$-values between 200 MeV/$c$ and 600 MeV/$c$, and for constant $q_\mu$ values between 200 MeV/$c$ and 500 MeV/$c$. A complete list of the corresponding values is available in ref. [37]).

## 7. Comparison with calculations

### 7.1. QUASIELASTIC PEAK

The cross sections and the longitudinal and transverse response functions have broad maxima at values of energy loss $\omega \simeq q_\mu^2/2M$ ($M$ is the nucleon mass); this is characteristic of the quasifree single-nucleon knock-out mechanism. We present the separated response functions for $q = 300$, 400 and 550 MeV/$c$ in figs. 9, 10, 11 and 12. In figs. 9 and 10, the experimental results are compared to relativistic Fermi-gas model calculations of Van Orden [8]). This model was chosen because of its conceptual simplicity but is only expected to be valid in the vicinity of the peak. One can see that the agreement is much better at the higher $q$-values (e.g. at 550 MeV/$c$). It is poor, especially for $R_L$, at lower $q$-values. Because the calculated transverse response tends to be too low and the longitudinal response too high, there is better agreement for the measured total cross sections than for the individual response functions.

A second calculation, shown in figs. 11 and 12, is due to Laget and Chrétien-Marquet [21]). These authors use a harmonic oscillator shell model which reasonably reproduces the momentum distributions obtained from the Saclay $^{12}$C(e, e'p) quasielastic coincidence experiment [22]). Final-state interactions were simulated with distorted waves derived from the real part of the same optical potential used in the (e, e'p) and ($\gamma$, p) experimental analyses [22,23]). This calculation is in better agreement with the experiment than is the Van Orden calculation. It works well for $R_L$, especially at high $q$, but always underestimates $R_T$.

### 7.2. DIP REGION

At high energy and momentum transfers the transverse response function dominates the scattering, in particular in (and above) the "dip region" between the quasielastic and resonant meson production peaks. This indicates that the excess strength previously reported in this region [1]) is predominantly transverse in nature. This feature is consistent with two-nucleon knock-out through a meson-exchange current (MEC) mechanism [24]) as indicated in the previous paper [3]) and as also reported in the $^{40}$Ca experiment of ref. [4]). Coherent pion electroproduction [25]) is estimated to be very small and cannot account for the excess strength.

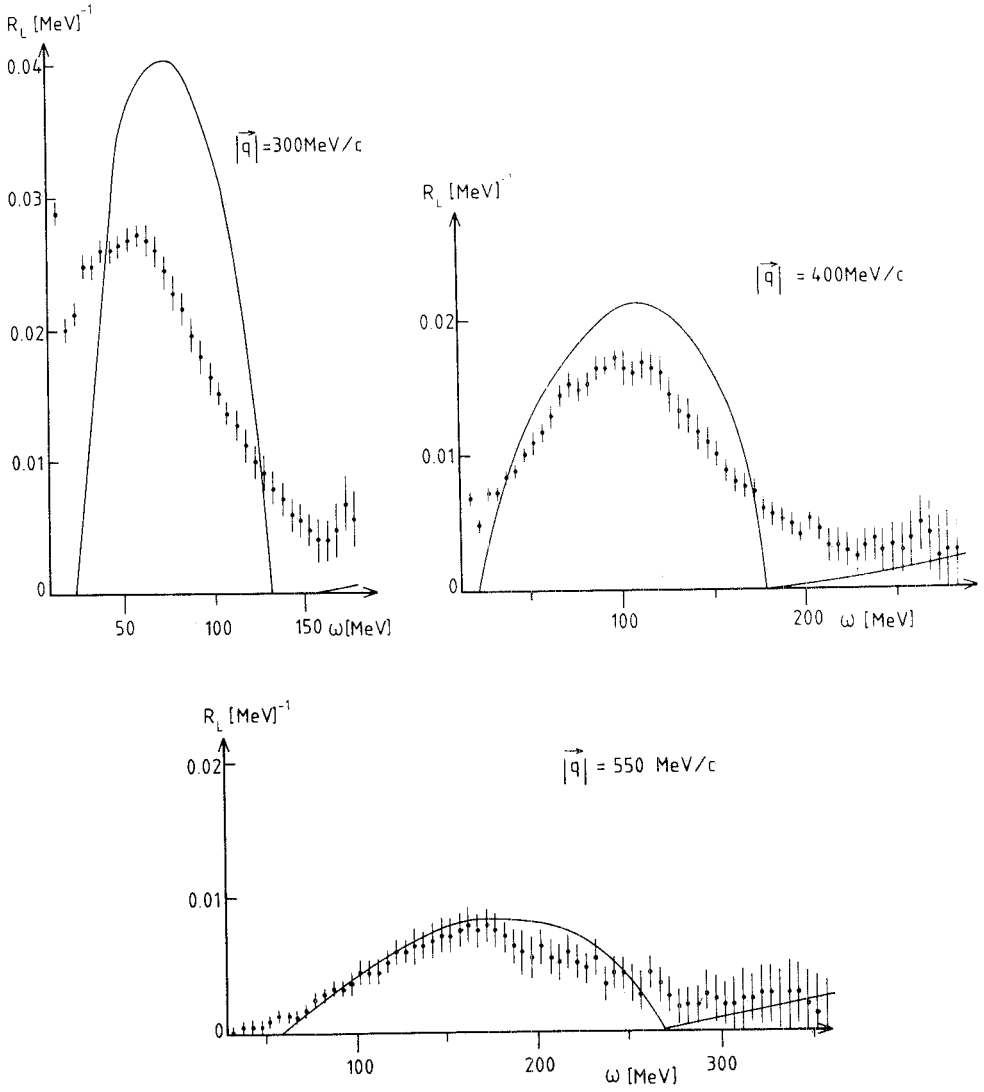


Fig. 9. The longitudinal response function $R_L$ versus $\omega$ for momentum transfer, $|\boldsymbol{q}|$, equal to (a) 300 MeV/$c$; (b) 400 MeV/$c$; (c) 550 MeV/$c$. Solid curves represent Fermi-gas calculations [refs. [8,26])]. In all the figures which follow, the solid curve represents the sum of the component curves: — — — quasielastic; · · · · · MEC; – – – pion production.

Several estimates of MEC contributions are shown in figs. 9–12. In their calculations, Donnelly and Van Orden use the Fermi gas model [26]), while Laget and Chrétien-Marquet [21]) use the quasi-deuteron model (fig. 13). The introduction of MEC reduces the differences between data and theory in the dip region. The overall agreement with the data is better for the shell model than for the Fermi-gas model. This occurs in part because in the latter the high-energy loss part of the quasielastic

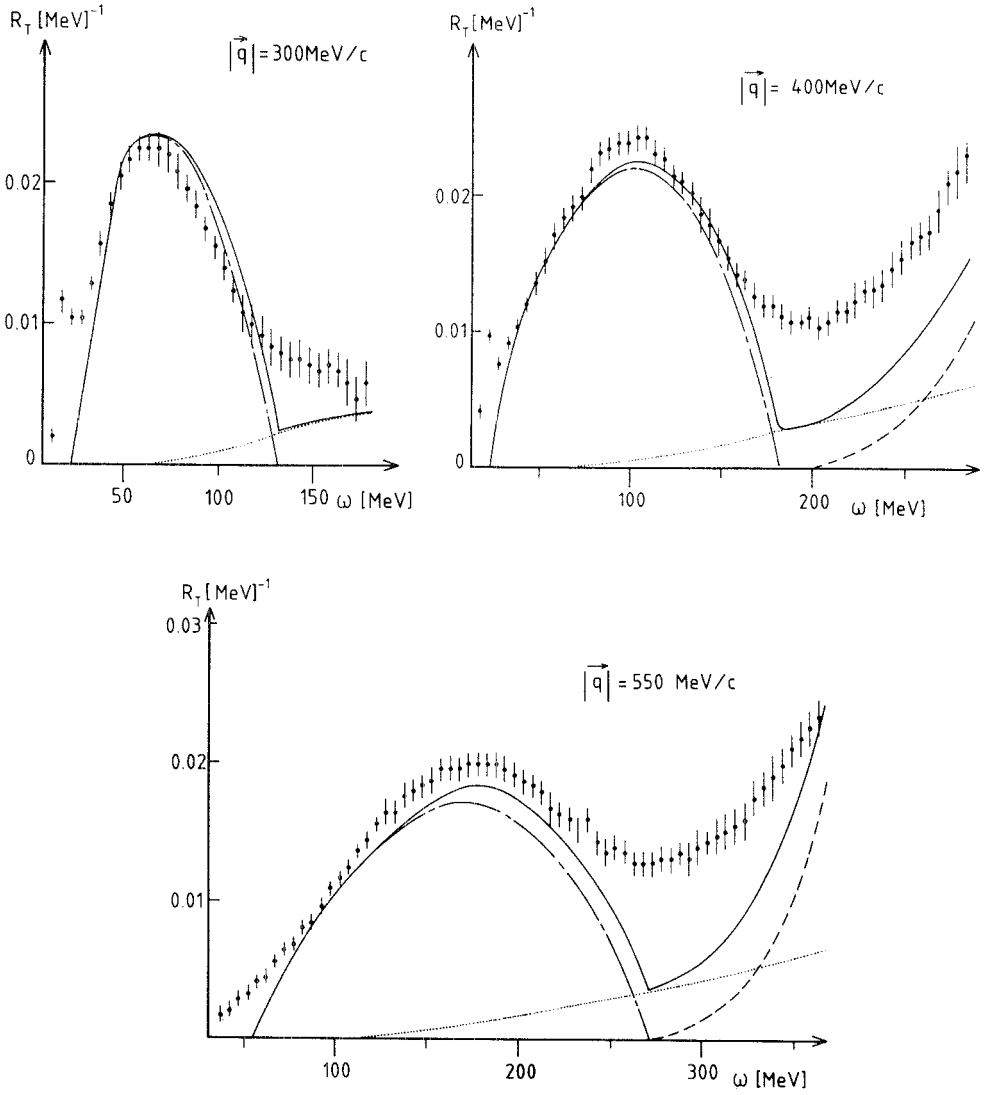


Fig. 10. The transverse response function $R_T$ versus $\omega$ for momentum transfer, $|q|$, equal (a) 300 MeV/$c$; (b) 400 MeV/$c$; (c) 550 MeV/$c$. Curves represent Fermi-gas calculations [refs. [8,24,26])]. See fig. 9.

peak is cut off too sharply due to the absence of initial nucleon momenta above the Fermi momentum.

## 8. Pion electroproduction

At higher $\omega$-values, pion production dominates the cross section. Near the pion production threshold, non-resonant terms [27]) are the most important; at larger $\omega$

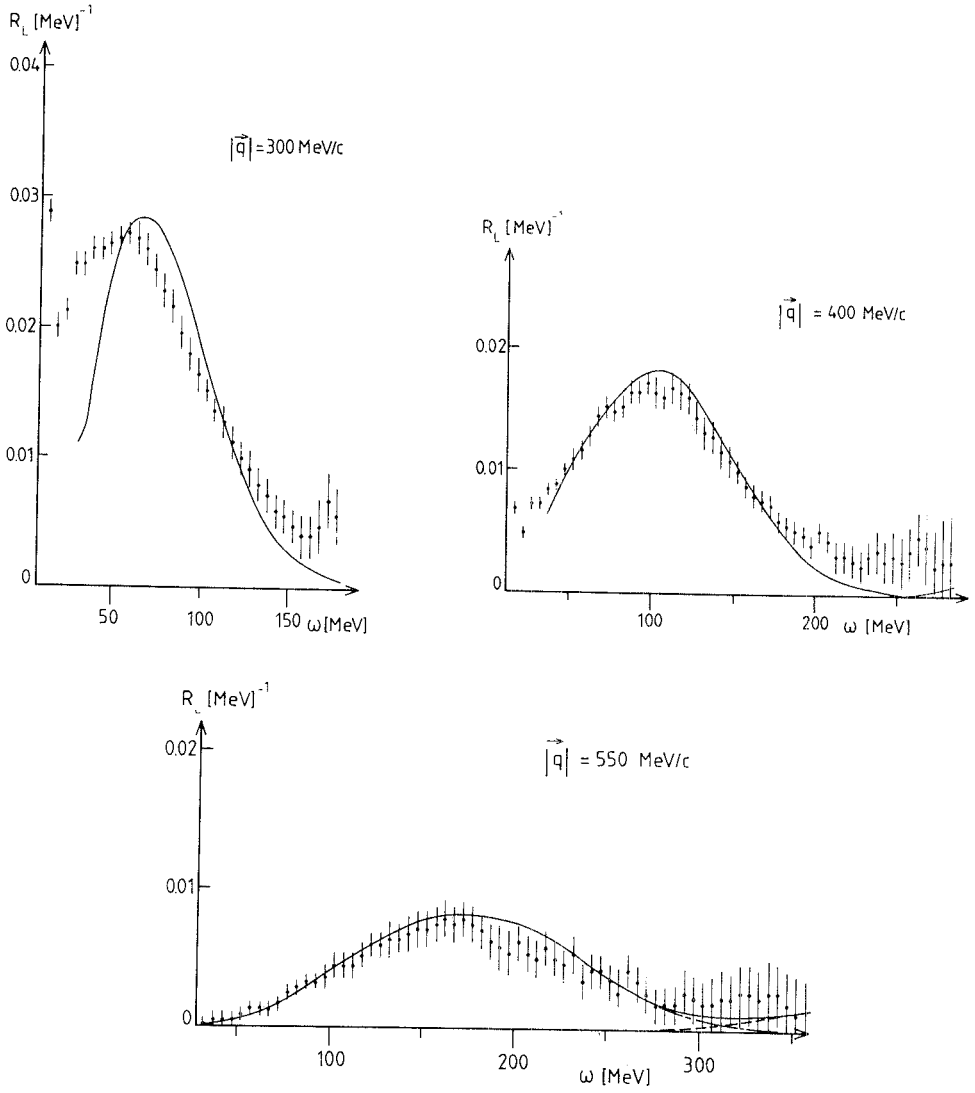


Fig. 11. Same as for fig. 9, except that curves are from shell-model calculations of refs. [21,29]).

the $\Delta$-resonance is the largest contribution to the cross section. Fig. 14 shows the results obtained at 680 MeV and 36°. It can be seen that the position of the experimental resonance is 30 MeV lower than that of the free nucleon resonance. This is also true for real photons [28]) as shown in fig. 15. However at 60°, i.e. at a higher momentum transfer, the position of the experimental resonance is closer to that of the free one (fig. 16).

Several models have been used to compute real pion electroproduction. Laget [29]) has made a quasi-free calculation (resonant and non-resonant terms) taking into

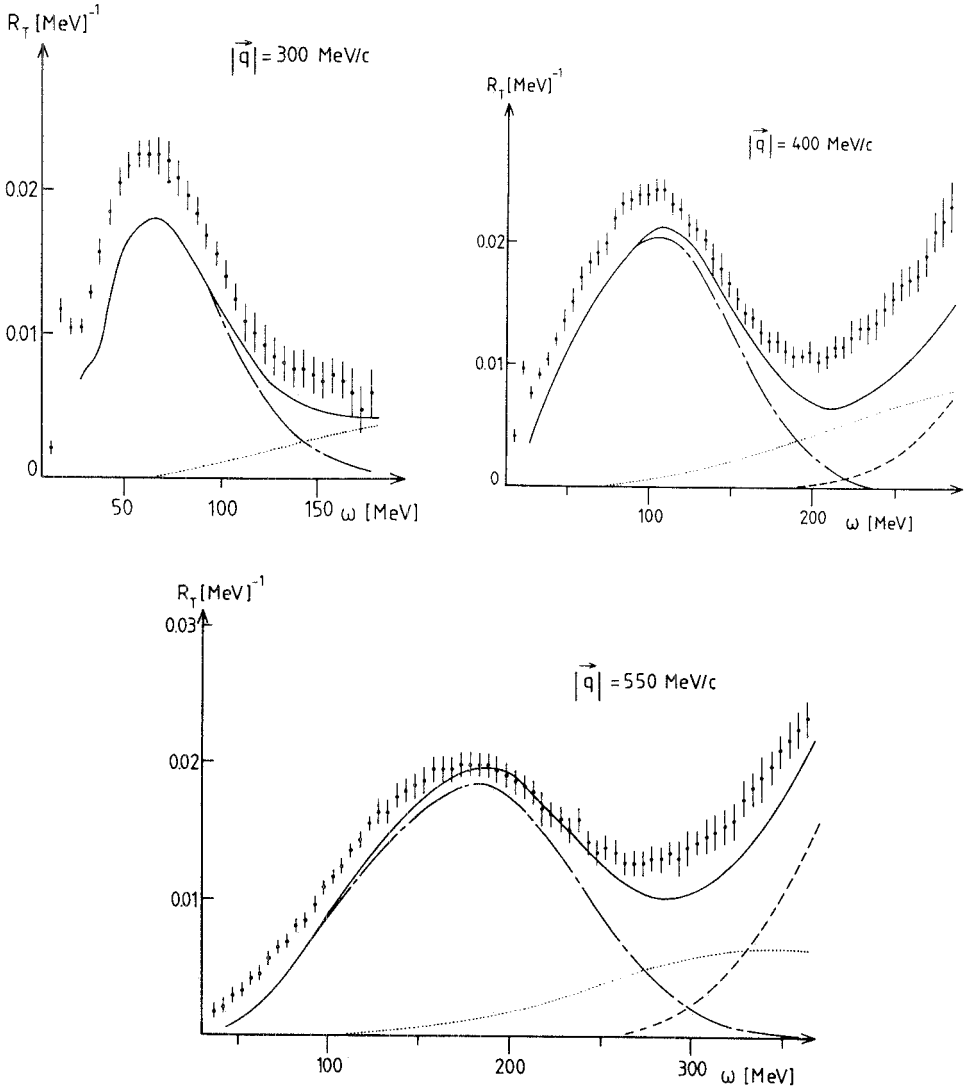


Fig. 12. Same as for fig. 10, except that curves are from refs. [21,29]).

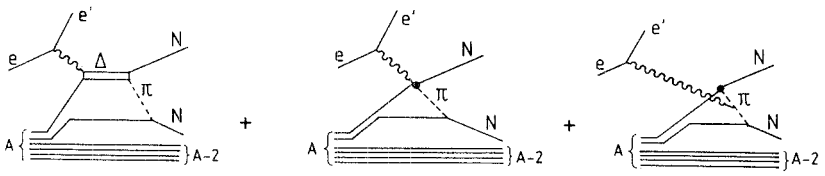


Fig. 13. Diagrams indicating two-nucleon (quasi-deuteron) contributions included in the calculations of Laget.

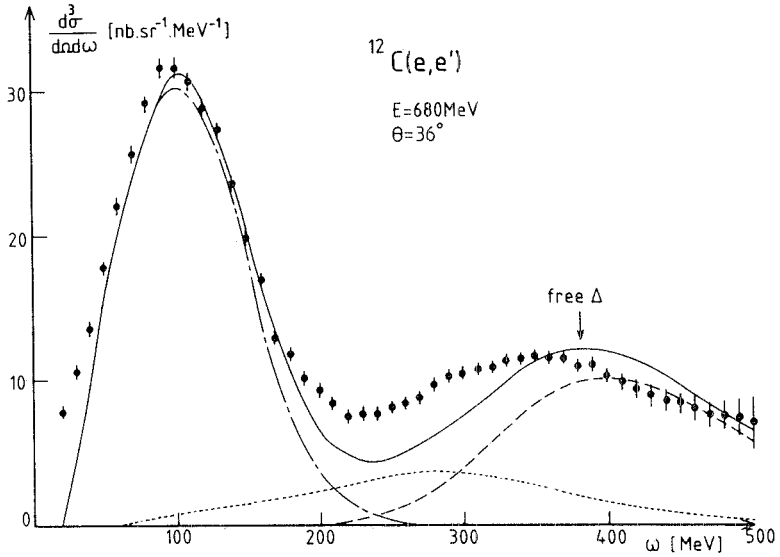


Fig. 14. Laboratory differential cross sections at forward angle $\theta = 36°$ as a function of $\omega$. The curves represent calculations by Laget and Chrétien-Marquet.

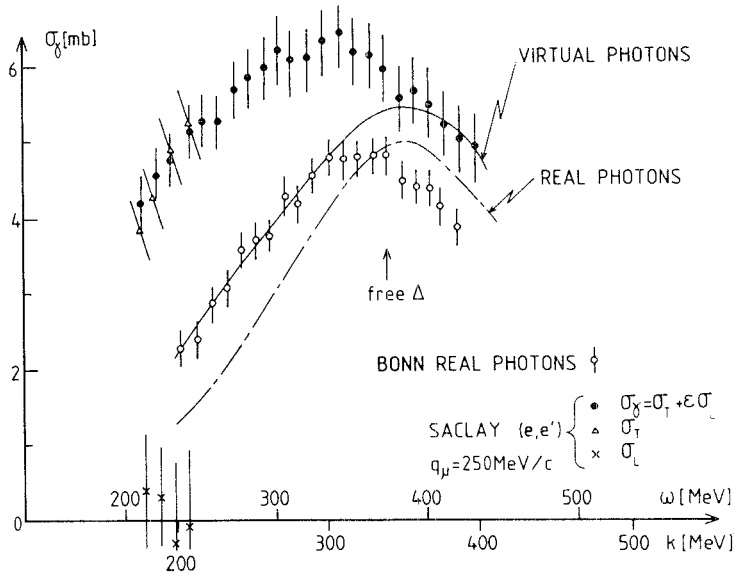


Fig. 15. Virtual and real photoabsorption cross sections as a function of $\omega$ (virtual photon energy) or $k$ (real photon energy). The virtual points are those of Saclay $^{12}$C(e, e') for $q_\mu = 250$ MeV/$c$ (present work). The real photon points are those of ref. [28]). The curves represent the Laget calculation [21,29]). For explanation concerning $\sigma_\gamma$, $\sigma_T$ and $\sigma_L$, see text subsect. 8.1.

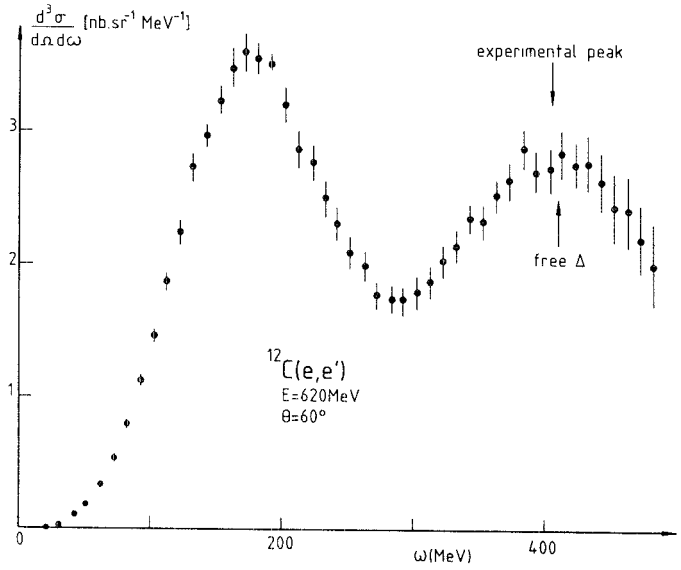


Fig. 16. Laboratory differential cross sections as function of $\omega$.

account the binding energy and the Fermi motion of the struck nucleon in the initial nucleus. His fit is fairly good at backward angles (fig. 17); at forward angles (fig. 14), his results in the dip region lie below those of the experiment, and the $\Delta$-peak appears at an energy loss higher than the experimental value.

The interaction of the $\Delta$ with the final nucleus has been studied by a number of authors. Do Dang [30]) describes the interaction by a central well potential whose

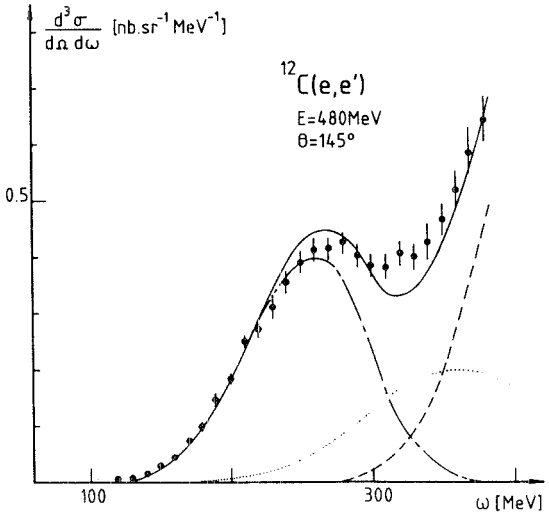


Fig. 17. Same caption as fig. 14, but at backward angle $\theta = 145°$.

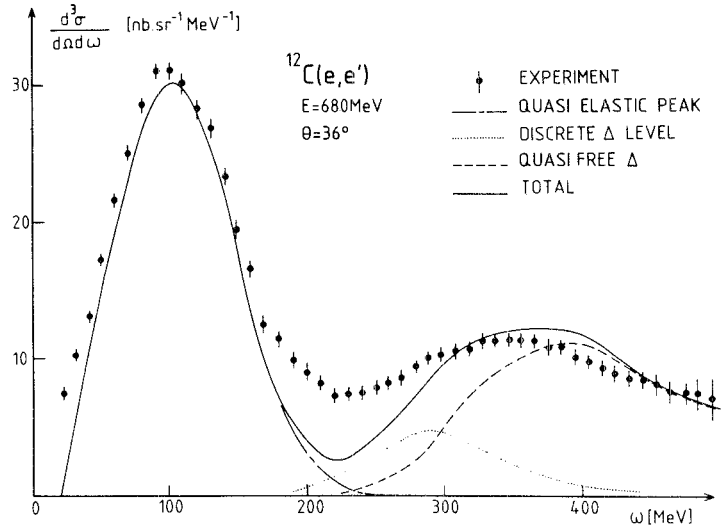


Fig. 18. Same as fig. 14. Calculations by Do Dang [30]).

depth is comparable to the nucleon–nucleus interaction (≈40 MeV). Figs. 18 and 19 show how his results compare with experiment. In the dip region the calculated cross section remains below the experimental one, especially at backward angles. Klingenbeck and Huber [31]) consider Δ-nucleus resonances of different multipolarities formed by Δ-hole excitations; figs. 20 and 21 show their results for two different angles; the agreement is good at forward angles but deteriorates at backward angles.

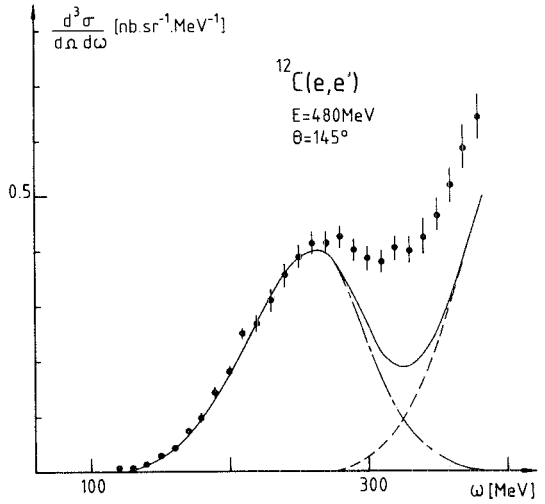


Fig. 19. Same as for fig. 17. Calculations by Do Dang [30]).

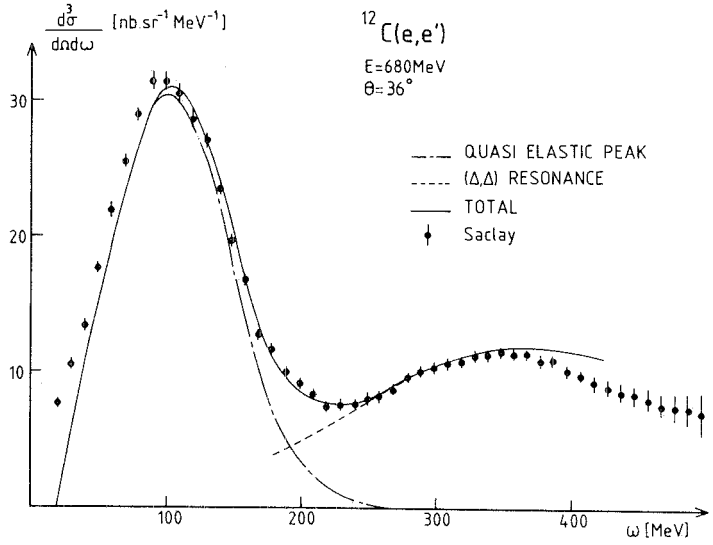


Fig. 20. Same as for fig. 14. Calculations by Klingenbeck and Huber [31]).

## 8.1. COMPARISON WITH REAL PHOTONS

It is convenient to rewrite the electron-scattering cross section (eq. (1)) in the form [20])

$$\frac{d^3\sigma}{d\Omega\, d\omega} = \Gamma(E, E', \theta)\sigma_\gamma(q, \omega)\,, \tag{2}$$

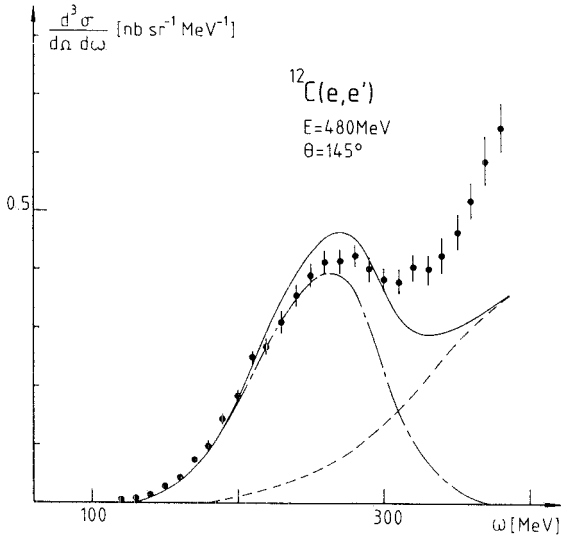


Fig. 21. Same as for fig. 17. Calculations by Klingenbeck and Huber [31]).

where

$$\sigma_\gamma(q,\omega)=\varepsilon\sigma_L(q,\omega)+\sigma_T(q,\omega)\,,$$

$$\Gamma(E,E',\theta)=\frac{\alpha}{4\pi^2}\frac{k}{q_\mu^2}\frac{E'}{E}\frac{2}{1-\varepsilon}\,,$$

$$\sigma_L(q,\omega)=\frac{4\pi^2}{k}\alpha\left(\frac{q_\mu}{q}\right)^2 R_L(q,\omega)\,,$$

$$\sigma_T(q,\omega)=\frac{2\pi^2}{k}\alpha R_T(q,\omega)\,.$$

$k$, a factor which cancels in eq. (2), is taken to be the energy of a real photon ($q_\mu^2\equiv 0$) which, when absorbed by a nucleon of mass $M$, creates an excited state of (invariant) mass $W$:

$$k=\frac{W^2-M^2}{2M}=\omega-\frac{q_\mu^2}{2M}\,.$$

The factor $\Gamma$ can be interpreted as the number of virtual photons/electron emitted in the $q$-direction per unit solid angle and energy loss. The polarization of the virtual photon is given by $\varepsilon$, previously introduced. $\sigma_L$ and $\sigma_T$, which have the dimensions of cross sections, are convenient for purposes of comparing the quasielastic scattering to the total photon-absorption cross sections.

In fig. 15, we can compare the real photon total absorption cross section measured at Bonn [28]) and $\sigma_\gamma(q,\omega)$ at $q_\mu=250$ MeV/$c$, extracted from our electroproduction measurements for $k>207$ MeV. This is justified for two reasons; first, in this region (i.e. $\omega>240$ MeV) the contribution of the quasielastic peak is negligible, as can be seen in fig. 14; second, the longitudinal part of the cross section is very small, as shown for lowest energy loss points of fig. 15 where the longitudinal/transverse decomposition could be performed with our data. The cross sections for virtual photons ($q_\mu^2>0$) are greater than for real photons, and the peak does not occur at the same value of $\omega$, although the shapes of the curves are similar. Fig. 22 shows the variation of $\sigma_\gamma$ versus $q_\mu^2$ for the value of $W$ near the maximum of the free $\Delta$ ($W=1236$ MeV). In that figure we have also plotted the real photon point measured at Bonn and the electroproduction data from Kharkov [32]); the present experiment is in excellent agreement with the Kharkov work. Using the multipoles for pion electroproduction on nucleons, Laget [21,29]) has calculated the electron cross sections on $^{12}$C for the kinematics of figs. 15 and 22. In fig. 22, one can see that for $k=345$ MeV, his calculation agrees with both the electron scattering and the real photon absorption measurements; the variation of the cross section to $q_\mu^2\to 0$ is not linear and does not validate a linear extrapolation to the real photon point. On the other hand, fig. 15 shows that the agreement of experiment and theory is good only for $k$-values $\geq 330$ MeV; a large discrepancy appears at low $k$-values.

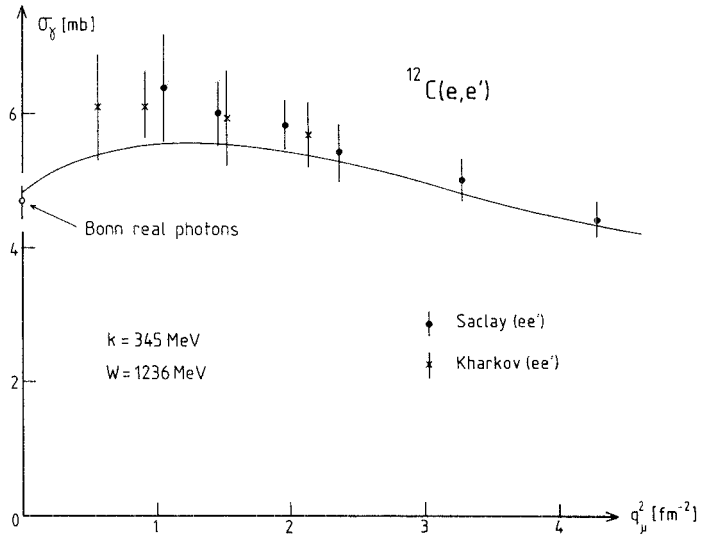


Fig. 22. Real and virtual photon absorption cross sections. The curve is due to Laget [21,29]).

## 9. Sum rule

It is possible to integrate the longitudinal response function with respect to $\omega$ at a given value of $q$. The result, often called a "sum rule" [6]) depends only on the nuclear ground-state properties and within the framework of a pure single-particle model of the nucleus, provides information about nucleon correlations. A true sum rule, however, results from an integral over all values of $\omega$, while in real experiment, $\omega \leqslant q$. For this reason, the experimentally determined integral can only approximately represent the sum-rule value. Furthermore, reliable experimental data cannot be obtained near the limit $\omega = q$ because of the presence of radiative corrections, falling detector efficiencies, and other technical considerations. In order to compare our data with the integral of the (theoretical) longitudinal response functions, we have evaluated the integral

$$\int_{\omega_{\min}}^{\omega_{\max}} R_{\mathrm{L}}(q, \omega)\, \mathrm{d}\omega$$

using the experimental values of $R_{\mathrm{L}}(q, \omega)$. In general, assuming a spectator model,

$$\omega = E_{\mathrm{m}} + \frac{p_{\mathrm{in}}^2}{2M_{A-1}} + [(\boldsymbol{p}_{\mathrm{in}} + \boldsymbol{q})^2 + M^2]^{1/2} - M,$$

where

$$E_{\mathrm{m}} \equiv M_{A-1}^{*} + M - M_A,$$

and $p_{\mathrm{in}}$ is the initial proton momentum. We have chosen $\omega_{\max}$ to correspond to a

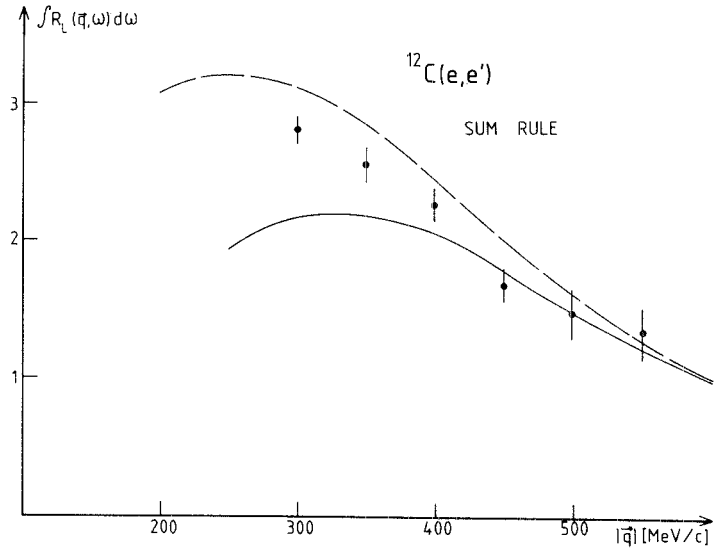


Fig. 23. Sum rule: the solid curve is due to Laget [21]), and the dashed curve is from Van Orden [8]).

value of $p_{in}$ equal to 300 MeV/$c$ in the direction of $q$ and have taken $E_m$ to equal 23 MeV, the average value determined from $^{12}$C(e, e'p) work [22]). $\omega_{min}$ was chosen to just exclude the elastic peak.

The integrated results are presented in fig. 23. The theoretical curves correspond to the calculations of Van Orden and of Laget. One can see that at high momentum transfers, the experimental integral agrees with the independent particle model calculation within the experimental error bars, approximately 10%. This corresponds to the maximum contribution of short-range correlations in the Coulomb sum rule as evaluated by Viollier and Walecka [33]). Our results significantly differ from that obtained by Altemus *et al.* [7]) for $^{56}$Fe, who find, for $q < 410$ MeV/$c$, an experimental integral 40% lower than is given by a Fermi-gas calculation. One can remark that in the $^{56}$Fe experiment the longitudinal response function $R_L$ falls off sharply at high-energy losses, while in our experiment $R_L$ decreases smoothly as expected. At low $q$-values, rescattering and many-body break-up terms are not included in the Laget calculation, resulting in reduced cross sections. These terms are taken into account at higher values of $q$ by use of the closure approximation.

## 10. Conclusion

The quasielastic peak in inelastic electron scattering at momentum transfers $q$ above about 400 MeV/$q$ can be fairly well understood in terms of independent particle shell models which, because of their higher nucleon momentum content, fit the data better than the simpler Fermi-gas model. Yet, it is not clear that

elaborations of a shell model *per se* can lead to a satisfactory fit to the response functions. Additional ingredients, with the introduction of new parameters, would appear necessary to explain adequately the extent and magnitude of the tails of the quasielastic peak and its precise position. Refinements in final-state interaction calculations as proposed by Horikawa *et al.* [34])† might improve the fits. At small momentum transfers the agreement is poor as expected, because the details of the nuclear structure which play a major role there, are not taken into account.

In deep-inelastic electron scattering, a measure of the validity of one-body interaction models can be obtained by the degree to which the longitudinal sum rule is verified. We find good agreement here, indicating that missing features in the applied theory such as two-body interactions (i.e. NN correlation effects) contribute less than 10%. This contrasts with the result for $^{56}$Fe [ref. [7]], where such agreement is missing. We note that a recent shell-model calculation by De Forest [35]) yields theoretical cross-section values which are significantly larger than those given by the calculations of either Van Orden or Laget.

In the dip region between the quasielastic peak and the $\Delta$-resonance peak, meson effects play an important role. Theory which uses a quasi-deuteron model improves the agreement with experiment, but is still not sufficient to explain the magnitudes of the observed cross sections. Other effects involving the nature of the $\Delta(1232)$ nucleon resonance in a nuclear medium can be invoked [36]) to fit the data, but at the present state of affairs do not offer a successful comprehensive explanation for all kinematical situations. In general, the $\Delta$-peak is at smaller energy loss than is predicted by quasi-free nucleon models, and seems to be wider than is predicted. A more complete approach to the nature of $\Delta$ production and propagation in nuclei would seem desirable.

Clues to the understanding of these complicated two-body effects can probably be more readily obtained by studying simpler nuclei whose specifically nucleonic dynamics are more adequately described.

It is a pleasure to thank Dr. L. Chrétien-Marquet, Dr. M. Danos, Dr. G. Do Dang, Dr. T.W. Donnelly, Prof. M. Huber, Dr. K. Klingenbeck, Dr. J.M. Laget and Prof. J.W. van Orden for their assistance, and for many useful conversations. We thank the staff of the ALS for their support. The visitors to Saclay especially thank the Laboratory for its hospitality.

## References

1) R.R. Whitney, I. Sick, J.R. Ficenec, R.D. Kephart and W.P. Trower, Phys. Rev. **C9** (1974) 2230
2) D. Day, J.S. McCarthy, I. Sick, R.G. Arnold, B.T. Chertok, S. Rock, Z.M. Szalata, F. Martin, B.A. Mecking and G. Tamas, Phys. Rev. Lett. **43** (1979) 1143;
J.S. McCarthy, I. Sick, R.R. Whitney and M.R. Yearian, Phys. Rev. **C13** (1976) 712

† The Saclay results quoted in this paper were preliminary and some cross sections were modified in the final analysis, especially the 401 MeV 60° cross sections.

3) J. Mougey, M. Bernheim, D. Royer, D. Tarnowski, S. Turck, P.D. Zimmerman, J.M. Finn, S. Frullani, D.B. Isabelle, G.P. Capitani, E. de Sanctis and I. Sick, Phys. Rev. Lett. **41** (1978) 1645
4) P.D. Zimmerman, J.M. Finn, C.F. Williamson, T. de Forest and W.C. Hermans, Phys. Lett. **80B** (1978) 45
5) I. Sick, D. Day and J.S. McCarthy, Phys. Rev. Lett. **45** (1980) 871
6) K.W. McVoy and L. van Hove, Phys. Rev. **125** (1963) 1034
7) R. Altemus, A. Cafolla, D. Day, J.S. McCarthy, R.R. Whitney and J.E. Wise, Phys. Rev. Lett. **44** (1980) 965;
R. Altemus, Ph.D. dissertation, University of Virginia, 1980, unpublished
8) J.W. Van Orden, Ph.D. dissertation, Stanford University, 1978, unpublished, and private communication
9) P. Leconte, J. Mougey, A. Tomasso, P. Barreau, M. Bernheim, A. Bussière, L. Cohen, J.-C. Comoretto, J. Dupont, S. Frullani, C. Grunberg, J.-M. Hisleur, J. Le Dévéhat, M. Lefèvre, G. Lemarchand, J. Millaud, D. Royer and R. Salvaudon, Nucl. Instr. **169** (1980) 401
10) M. Cantin, M. Casse, L. Koch, R. Jouan, P. Mestreau, D. Roussel, F. Bonnin, J. Moutel and S.J. Teichner, Nucl. Instr. **118** (1974) 177
11) L.S. Cardman, J.W. Lightbody Jr., S. Penner, S.P. Fivozinsky, X. K. Maruyama, W.P. Trower and S.E. Williamson, Phys. Lett. **91B** (1980) 203
12) W. Reuter, G. Fricke, K. Merle and H. Miska, Phys. Rev. **C26** (1982) 806
13) G. Miller, SLAC Report no. 129 (1971)
14) Y.S. Tsai, SLAC-PUB-848, Jan. 1971
15) L.W. Mo and Y.S. Tsai, Rev. Mod. Phys. **41** (1969) 205
16) C. Chahine, Phys. Rev. **D22** (1980) 1062; 2727
17) C.W. de Jager, H. DeVries and C. DeVries, Atom. Nucl. Data Tables **14** (1974) 479
18) E. Borie, Lett. Nuovo Cim. **1** (1971) 106
19) J. Berthot and D.B. Isabelle, J. Phys. App. **7** (1972) 413
20) C.W. Akerlof, W.W. Ash, K. Berkelman, A. Lichtenstein, A. Ramanausk'as and R.H. Siemann, Phys. Rev. **163** (1967) 1482
21) J.M. Laget, From collective states to quarks in nuclei, Lecture Notes in Physics vol. 137, ed. H. Arenhövel and A.M. Saruis (Springer, Berlin, 1981) p. 148, and private communication;
L. Chrétien-Marquet, Thèse 3ème cycle, 1981, unpublished
22) J. Mougey, M. Bernheim, A. Bussière, A. Gillebert, Phan Xuan Ho, M. Priou, D. Royer, I. Sick and G.J. Wagner, Nucl. Phys. **A262** (1976) 461
23) D.J.S. Findlay, R.O. Owens, M.J. Leitch, J.L. Matthews, C.A. Peridier, B.L. Roberts and C.P. Sargent, Phys. Lett. **74B** (1978) 305
24) T.W. Donnelly, J.W. Van Orden, T. de Forest Jr. and W.C. Hermans, Phys. Lett. **76B** (1978) 393
25) E. Borie, Proc. of the 7th ICOHEPANS, Zurich (Switzerland) (1977) 247
26) J.W. Van Orden and T.W. Donnelly, Ann. of Phys. **131** (1981) 4
27) G.F. Chew, M.L. Goldberger, F.E. Low and Y. Nambu, Phys. Rev. **106** (1957) 1345
28) J. Arends, J. Eyink, A. Hegerath, K.G. Hilger, B. Mecking, G. Noldeke and H. Rost, Phys. Lett. **98B** (1981) 423;
J. Ahrens, Nucl. Phys. **A335** (1980) 67
29) J.M. Laget, Phys. Reports **69** (1981) 1; Nucl. Phys. **A358** (1981) 275C
30) G. Do Dang, Z. Phys. **A294** (1980) 377
31) K. Klingenbeck and M.G. Huber, Phys. Rev. **C22** (1980) 681
32) V.G. Vlasenko, V.A. Goldstein, A.V. Mitrofanova, V.I. Noga, Yu.N. Ranuuk, V.I. Startsev, P.V. Sorokin and Yu.N. Telegin, Sov. J. Nucl. Phys. **23** (1976) 265
33) R.D. Viollier and J.D. Walecka, Acta Phys. Polon. **B8** (1977)
34) Y. Horikawa, P. Lenz and Nimai C. Mukhopadhyay, Phys. Rev. **C22** (1980) 1680
35) T. de Forest, private communication
36) E. Moniz, Electron and pion interaction with nuclei at intermediate energies, ed. W. Bertozzi, S. Costa and C. Schaerf (Harwood Academic Publishers, 1980) p. 475
37) P. Barreau, M. Bernheim, J. Duclos, J. M. Finn, Z. Meziani, J. Morgenstern, J. Mougey, D. Royer, B. Saghai, D. Tarnowski, S. Turck-Chieze, M. Brussel, G. P. Capitani, E. de Sanctis, S. Frullani, F. Garibaldi, D. B. Isabelle, E. Jans, I. Sick and P. D. Zimmerman, Note CEA N-2334